Strain-induced band modulation of thermal phonons in carbon nanotubes

Masato Ohnishi and Junichiro Shiomi*

Department of Mechanical Engineering, The University of Tokyo, Hongo 7-3-1, Bunkyo-ku, Tokyo 113-8656, Japan

(Received 9 April 2019; revised 15 April 2021; accepted 1 June 2021; published 16 July 2021)

We show that carbon nanopeapods are an ideal artificial superlattice to induce band modulation of thermal phonons. Based on spectral energy density analysis, we found that a periodic deformation in carbon nanotubes induced by fullerene encapsulation leads to zone folding of phonon dispersions up to near the maximum frequency. The zone-folding effect gives rise to phonon band gaps caused either by Bragg reflection or mode hybridization, and this reduces group velocity. This was quantified to play the leading role in reduction of thermal conductivity by the fullerene encapsulation. The strain modulation of thermal phonon bands opens a possibility to control material thermal conductivity.

DOI: 10.1103/PhysRevB.104.014306

Heat conduction can be manipulated by taking advantage of the particle [1] and wave [2] nature of phonons [3]. When a characteristic size of nanostructures such as grain size [1,4] and distance between pores [5] is comparable with or less than phonon mean-free-paths (MFPs), e.g., on the order of 10 nm to 10 μm for silicon at room temperature [6], nanostructures enhance phonon scattering and reduce thermal conductivity of the materials. Another and more ambitious direction of phonon manipulation is based on wave nature [2]. Periodic structures can modulate phonon wave nature by, for example, generating phonon gaps [7,8] and may realize low thermal conductivity for thermoelectric devices and thermal insulators or more advanced phonon engineering such as thermal rectification [9] and thermal cloaking [10,11]. While a recent study indicates that MFP is comparable with coherence length in ideal systems [12] because phonons easily lose their phase information due to disorders in materials such as surface roughness and impurities [13–18], coherent phonon effects can be observed only when a characteristic size of nanostructures reaches the order of phonon wavelength; that is to say, effective coherence length is on the order of phonon wavelength in practice. Therefore, the short wavelength of thermal phonons, e.g., 1–10 nm in silicon at room temperature, has made the fabrication of structures with a characteristic size shorter than coherence length difficult and limited the observation of band modulation of thermal phonons to only at low temperature ($<$10 K) [17] or at low frequency ($<$1 THz) [15]. While superlattices with a single-nanometer period and atomic-scale roughness may enable modulation of coherent wave nature of thermal phonons at room temperature [19], the presence of heterointerfaces disturbs their mutual adaptability, for instance, for electron transport for thermoelectric application. Recently, local phenomena of coherent phonons, resonance and hybridization in nanopillars or junctions [20–23], and localization due to disordered structures [24,25] have been proposed as more robust strategies to control phonon wave nature. However, the fabrication of these structures is also difficult [26] because their scale still needs to be on the order of coherence length.

Carbon nanopeapods (or simply called peapods), fullerene-encapsulated single-walled carbon nanotubes (SWNTs), may overcome the above problems because of their short ($\approx$1 nm) periodicity, which is sufficiently shorter than wavelengths of thermal phonons at room temperature, and the absence of interface along the carrier transport direction. For electron transport, it has been suggested that nanopeapods act as a superlattice generating electron gaps because of a periodicity of encapsulated fullerenes [27]. On the other hand, for thermal transport, underestimation of interlayer interaction between encapsulated fullerenes and outer SWNTs have misled the understanding of effects of the fullerene encapsulation [28,29]. A recent measurement of thermal properties of multiple SWNTs and peapods [30] has revealed that the fullerene encapsulation significantly reduces thermal conductivity of carbon nanotubes (CNTs) due to the interlayer interaction. Reference [30] also showed that the reduction can be attributed to radial expansion of outer SWNTs [27,30–32] causing modulation in the phonon dispersion such as phonon softening and zone folding, although the details are yet to be understood. In this paper, we show how the periodic strain field induced by the fullerene encapsulation modulates wave nature of thermal phonons of SWNTs. Based on molecular dynamics (MD) with spectral energy density (SED) analysis, we reveal that thermal conductivity decreases mainly due to wave interference effect, namely, zone-folding effect. The zone-folding effect can be observed up to near the maximum frequency ($\approx$40 THz), which is much higher than that for nanopillars and junctions proposed in previous studies ($\approx$1 THz) [20–23]. The knowledge in how induced strain can modulate phonon bands provides a way to tune thermal phonon properties, strain engineering of wave nature of thermal phonons.

In the MD calculations, (10, 10) SWNTs with the length of $\approx$250 nm (1024 primitive unit cells of the SWNT) are

*shiomi@photon.t.u-tokyo.ac.jp

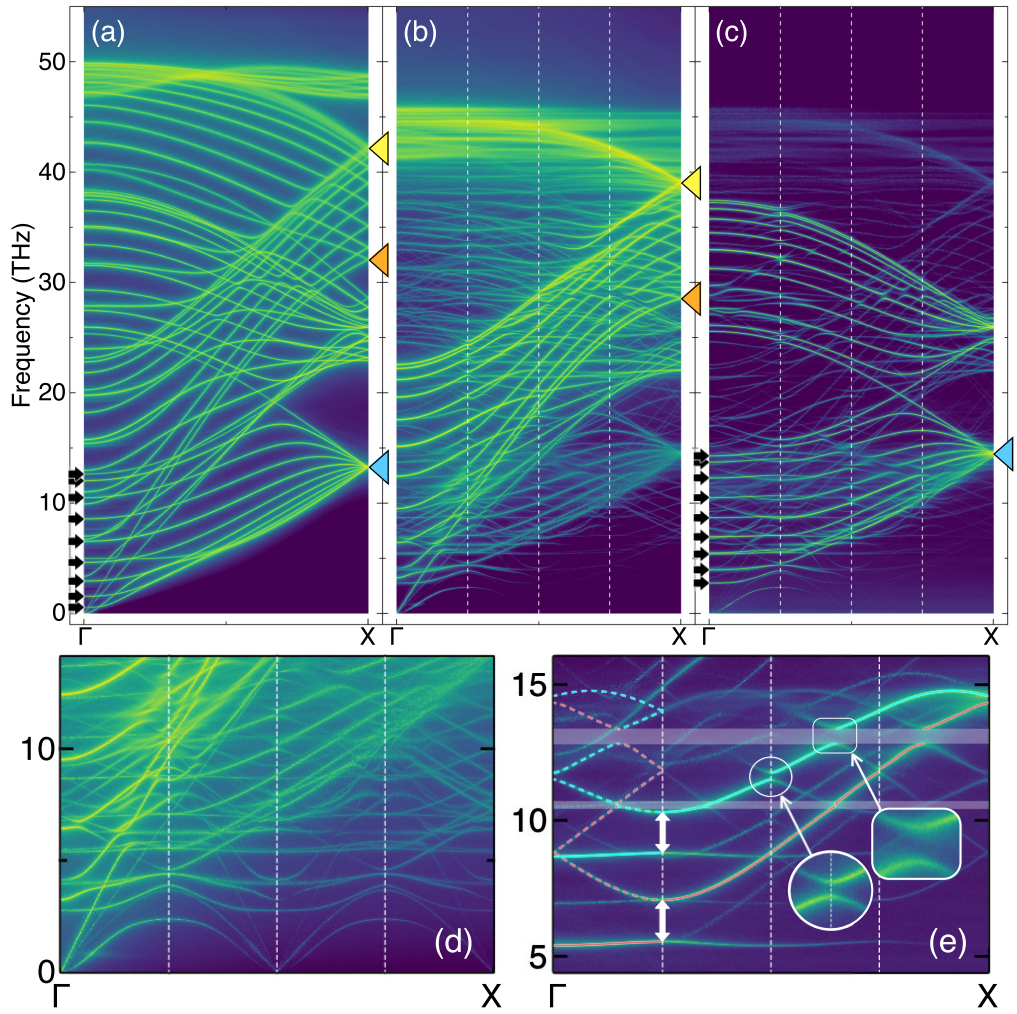

FIG. 1. Phonon dispersion of (a) a (10, 10) SWNT and (b)–(e) C_{60}@(10, 10) peapod; (b) axial modes, (c) radial modes, (d) axial modes in low-frequency region, and (e) radial modes with $q_\theta = 4$. (a)–(c) Arrows and markers show a band edge of representative bands for axial (yellow and orange) and radial (blue and black arrows) modes. (d) Symmetric bands due to a zone-folding effect can be clearly observed. (e) Phonon gaps at symmetric and asymmetric points show Bragg gaps and hybridization gaps induced by the zone-folding effect, respectively. Solid and dashed colored lines show, respectively, phonon bands tracing spectral energy density (SED) peaks and the corresponding folded bands in the Brillouin zone of the peapod. Vertical white dashed lines show symmetric points.

used, and a C_{60} fullerene is encapsulated in every four primitive unit cells of the SWNT (with ≈0.98 nm interval) in a peapod. Optimized Tersoff potential [33] and 12–6 Lennard-Jones potential are adopted to describe the covalent bonds and the intermolecular van der Waals interactions, respectively. The energy and length scales of the Lennard-Jones potential 2.4 meV and 5.0 Å have been determined to reproduce the experimentally observed deformation and reduction in thermal conductivity of peapods [30]. After the energy minimization with these interatomic potentials, the system is thermostated and equilibrated at 300 K in a canonical ensemble for 1 ns under a periodic boundary condition. After reaching the equilibrium state, velocities of individual atoms in the SWNT are recorded every 8 fs for 32 768 steps (≈260 ps) in total (see Table S1 in the Supplemental Material (SM) [34]). In every calculation, the time step is set to be 0.5 fs, and the temperature is controlled by Nosé-Hoover thermostat. By performing spatial and temporal Fourier transform with respect to the series of velocities taking advantage of the translational and 10-fold rotational symmetries of the SWNT [35,36], we obtained the SED of the SWNT and peapod. The translational wave vector and rotational wave number are denoted by q_z ($0 \leqslant q_z < 2\pi/a_{\rm lat}$ with $a_{\rm lat} = 2.5$ Å being the length of the primitive unit cell of the SWNT) and q_θ ($q_\theta = 0$ to 9), respectively. Forty independent simulations are performed with different randomized initial conditions to obtain a statistical average. It is worth mentioning that the MD method includes full anharmonicity, and thus, the issue of finite coherence length is intrinsically incorporated. Furthermore, it is suited for calculating soft materials, where the lattice forms far away from equilibrium positions, making perturbation analysis such as lattice dynamics less relevant.

Figure 1 shows the SED of (a) the (10, 10) SWNT and (b)–(e) the C_{60} peapod. The radial expansion due to the fullerene encapsulation leads to softening of axial modes [Fig. 1(b)] and hardening of radial modes [Fig. 1(c)], as indicated by markers in Figs. 1(a)–1(c) [30]. While softening of axial modes naturally results in decrease in phonon group velocity, the

hardening of radial modes also results in decrease of group velocity because hardening is stronger for longer wavelength phonons; the black arrows in Fig. 1(c) clearly show stronger flattening for radial modes with longer wavelength. Because a uniform radial expansion leads to a similar change in phonon dispersions [30], we can regard such strain effects, softening of axial modes and hardening of radial modes, as a uniform strain effect [37].

Another consequence of the radial expansion is a zone folding of phonon dispersion, a representative phenomenon of coherent interference of phonons. Figure 1(d) clearly shows that symmetric bands are generated by the zone-folding effect. Moreover, the zone-folding effect can be observed up to ≈40 THz (e.g., see Figs. 1(c) and S1 in the SM [34]), which is much higher frequency than for phonon resonance in nanopillar or nanojunction structures (⩽1 THz) [21–23]. Note that the coherence of phonons becomes more vulnerable to roughness or anharmonicity as frequency increases, and thus, the maximum frequency with zone-folding features is a measure of how fine the phonon interference has been realized. We can, therefore, expect to modulate thermal properties of CNTs by tuning phonon wave nature at room temperature with the fullerene encapsulation. Interestingly, the zone-folding effect induces two types of phonon gaps: gaps at symmetric points ($q_z a_{\rm lat}/\pi = 0.25i$, $i = 1, \ldots, 4$) and asymmetric points [see blow-ups in Fig. 1(e)]. Gaps at symmetric points are due to the Bragg effect. Particularly, phonon bands of long-wavelength radial modes are heavily flattened at $\omega < 15$ THz because of large Bragg gaps (up to 1.6 THz), as indicated by arrows in Figs. 1(c) and 1(e). While the zone-folding effect is remarkable for long-wavelength phonons ($q_z a_{\rm lat}/\pi = 0.25$), Bragg gaps are generated also for middle- and short-wavelength phonons ($q_z a_{\rm lat}/\pi = 0.5, 0.75, 1.0$). In addition to the Bragg gaps at symmetric points, we can find phonon gaps at asymmetric points in Fig. 1(c) (at $q_z a_{\rm lat}/\pi \approx 0.5$–$1.0$ and $\omega \approx$ 10–15 THz). To describe how these phonon gaps are generated, phonon dispersion of radial modes with $q_\theta = 4$ is shown in Fig. 1(e) as a typical example. Two distinct separated radial modes are present for each q_θ except for $q_\theta = n/2$ ($n = 10$). These bands originally do not interact with each other in the SWNT. The zone folding, however, makes them hybridize with each other as denoted with dashed bands in Fig. 1(e) and generate phonon gaps in both bands at the same frequency as highlighted by white bands. Consequently, because of the presence of Bragg gaps and hybridization gaps, the zone-folding effect decreases group velocity not only at long-wavelength phonons but also short-wavelength phonons.

Next, we extract relaxation time (τ) by fitting Lorentzian functions to the SED data. Figure 2 shows the obtained frequency dependence of relaxation time of (a) transverse acoustic (TA), (b) twisting acoustic (TW), (c) longitudinal mode (LA) and radial breathing mode (RBM), and (d) optical modes (also see Fig. S5 in the SM [34]). Detailed descriptions of how to extract phonon branches and evaluate the error can be found in Secs. 1 and 2 in the SM [34]. Because the total simulation duration (260 ps) which determines the frequency resolution of SED (3.8 GHz) is not sufficient for phonon modes with large relaxation times, we have carefully analyzed fitting errors with Lorentzian function. While details are described in Sec. 2 in the SM [34], it is worth briefly mentioning

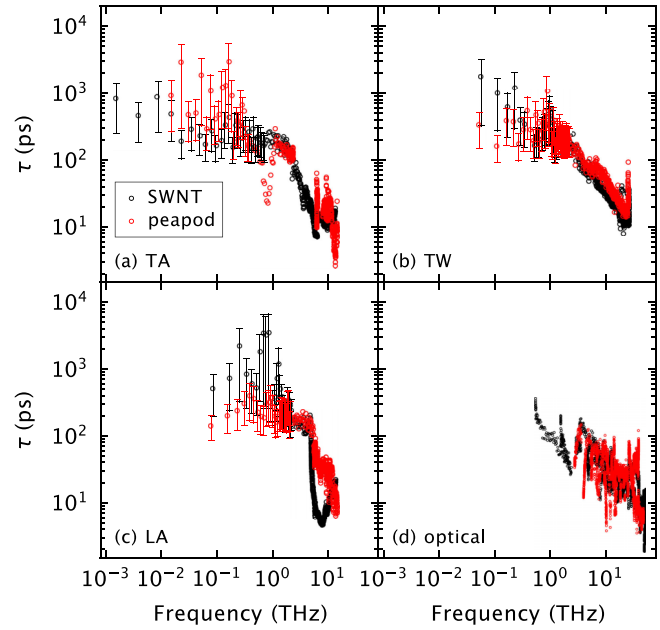

FIG. 2. Frequency dependence of phonon relaxation time of carbon nanotubes (CNTs). The data are assigned to (a) transverse acoustic (TA), (b) twisting acoustic (TW), (c) longitudinal acoustic (LA) and radial breathing mode (RBM), and (d) optical modes. Black and red markers are used for single-walled carbon nanotube (SWNT) and peapod, respectively. Error bars are shown only for data obtained with a local minimum of relaxation time (please see Sec. 2 in the Supplemental Material [34] for details of the error of relaxation time).

the process of the error analysis here. When the frequency resolution of SED is sufficiently fine, the peak frequency of the Lorentzian function can be determined by a coefficient of determination $R^2 = 1 - \sum (y_i - f_i)^2 / \sum (y_i - \bar{y})^2$, where y_i and f_i are the values of the SED and the Lorentzian function at the ith frequency, and $\bar{y}$ is the average value of the SED used for the fitting (see Fig. S2(b-i) in the SM [34]). However, determination of the peak frequency with R^2 leads to an extreme (a few orders of magnitude) overestimation of relaxation time for some cases of large relaxation time. We, therefore, employed a local minimum of relaxation times to determine relaxation time in such cases, as shown in Fig. S2(b-iii). In addition, we have estimated the error of extracted relaxation time as a function of the relaxation time: $|\varepsilon| = 0.38 \log \tau_0 - 0.41$, where $\varepsilon = (\tau - \tau_0)/\tau_0$ with τ and τ_0 being the extracted relaxation time and the true value, respectively (see Fig. S2(c) in the SM [34]). Note that τ_0 is replaced by τ in the following analysis because τ_0 is unknown. In Fig. 2, error bars obtained by this relation are shown only on data obtained with the local minimum of τ for the simplicity.

It is also worth comparing the simulation duration of the individual SED analysis, which is carried out under an equilibrium state, and the correlation time required in the framework of equilibrium MD with Green-Kubo formula. While a recent paper employed a long correlation time (2 ns), the thermal conductivity converged to a value within the statistical error in ∼250 ps [38]. The simulation duration in this analysis (260 ps) is reasonably long while an error analysis was required.

As for the obtained phonon properties, it is interesting that the relaxation time increases due to the fullerene encapsulation for some modes (particularly for low-frequency LA modes and high-frequency TA modes); although, as shown in Fig. S5(b) in the SM [34] and will be quantified later, the extent of increase is outcasted by the reduction in the group velocity. While a detailed analysis is difficult with the SED analysis, it may be possible to ascribe the increase in relaxation times to the flexibility of SWNT. From the perspective of the phonon, the flexibility of SWNT can be considered as long-wavelength transverse modes with large amplitudes, which induce local strain fields, as shown in Fig. S6 in the SM [34]. Because the local strain field affects transport of short-wavelength longitudinal modes, the flexibility finally results in interaction between these transverse and longitudinal modes and to reduction of their relaxation times. On the other hand, these phonon modes do not significantly interact with each other in the rigid system, peapod, and thus, their relaxation times increase because of the fullerene encapsulation. More discussion and Fig. S6 can be found in Sec. 4 in the SM [34].

Using extracted group velocity and relaxation time, we calculate thermal conductivity with the Boltzmann transport equation: $\kappa = \sum_{q_z,s} \kappa(q_z,s) = (\frac{k_B}{V}) \sum_{q_z,s} v_g^2(q_z,s)\tau(q_z,s)$, where k_B is Boltzmann constant, V is the CNT volume with a hexagonal cross section [30], and s is phonon branch. Thermal conductivity decreases from $\kappa_{\rm sw} = 2500$ to $\kappa_{\rm pea} = 1800\,{\rm Wm^{-1}\,K^{-1}}$ (29%) due to the fullerene encapsulation, where "sw" and "pea" denote SWNT and peapod, respectively. The errors of the calculated thermal conductivity were estimated as 20 and 16% for the SWNT and peapod, respectively, as discussed in Sec. 2 in the SM [34]. Thermal conductivity obtained in this evaluation should be a length-convergent value because it converges with the CNT length of 10–20 nm in equilibrium MD simulations with the Green-Kubo formula [39–41] (also see the discussion in Sec. 3 in the SM [34]). The thermal conductivity of the SWNT obtained in this paper ($2500\,{\rm Wm^{-1}\,K^{-1}}$) was, indeed, in good agreement with the converged value for the (10, 10) SWNT obtained with the Green-Kubo formula ($2200\,{\rm Wm^{-1}\,K^{-1}}$) [38].

It would also be worthwhile to compare with values in the previous work [30]. While a thermal conductivity calculated with a nonequilibrium MD (NEMD) simulation was $220\,{\rm Wm^{-1}\,K^{-1}}$ for (10, 10) SWNT, which is 10 times smaller than the value obtained in this paper, the SWNT used in the NEMD simulation contains adiabatic layers and thermostats at both ends, resulting in phonon scattering. The SWNT used in the NEMD simulation consists of a 40 nm center region connected with 20 nm thermostats which are terminated by adiabatic layers. Phonon MFPs in the SWNT for the NEMD simulation are, therefore, limited at 40–80 nm. To include the length effect, which is absent in the SED analysis, phonon scattering rates were calculated by Matthiessen's rule $\tau_{\rm tot}^{-1} = \tau_{\rm pp}^{-1} + \tau_{\rm bdy}^{-1}$, where phonon-phonon scattering rate ($\tau_{\rm pp}^{-1}$) was obtained from the SED analysis, and boundary scattering rate was calculated as $\tau_{\rm bdy}^{-1} = 2v_g/L_{\rm cnt}$ with $L_{\rm cnt}$ being the CNT length. Finally, the estimated thermal conductivity was 200–$350\,{\rm Wm^{-1}\,K^{-1}}$ for $L_{\rm cnt} = 40-80$ nm, which is consistent with the previous NEMD simulation.

We also compare the thermal conductivity obtained with the SED analysis with an experimentally obtained value

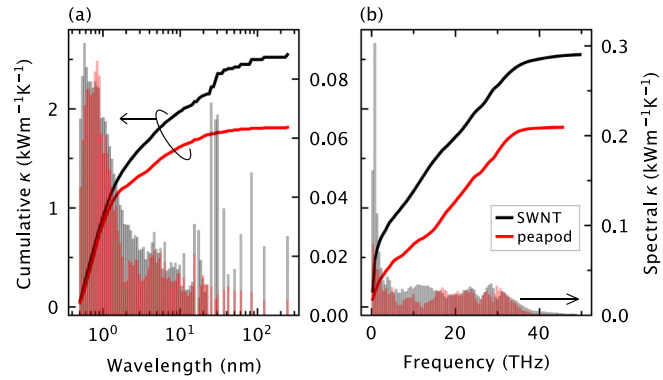

FIG. 3. Thermal conductivity of the single-walled carbon nanotube (SWNT; black) and peapod (red) with respect to phonon (a) wavelength and (b) frequency. The solid lines and filled curves show, respectively, cumulative and spectral thermal conductivity.

$200\,{\rm Wm^{-1}\,K^{-1}}$ for 1 μm SWNT bundles [30]. To additionally consider the effect of interlayer interaction between tubes in a CNT bundle, a term for phonon scattering between tubes $\tau_{\rm tt}^{-1}$ was added in the above Matthiessen's rule. This term was assumed not to depend on the phonon mode (phonon frequency and polarization) and was determined to reproduce the experimental value. Finally, the experiment value of SWNT bundles ($200\,{\rm Wm^{-1}\,K^{-1}}$) could be reproduced with $\tau_{tt}^{-1} = 0.41$ THz, which was in the same order of scattering rate due to silicon substrate [36]. Furthermore, thermal conductivity of the peapod estimated using the determined $\tau_{\rm tt}^{-1}$ was $125\,{\rm Wm^{-1}\,K^{-1}}$, which is 37% smaller than that of the SWNT. This estimation indicates that the reduction of thermal conductivity may appear stronger when other factors enhance phonon scattering in both systems, SWNT and peapod. Finally, we would also like to mention hydrodynamics phonon transport in SWNT. While in carbon-based materials effects of hydrodynamic phonon transport have nonnegligible contribution to heat transport [42–45], its effect should be negligible in CNTs except for CNTs with long length (>10 μm) and large diameter (>2.7 nm) below room temperature [46].

Cumulative and spectral thermal conductivity reflects features of zone-folding effects. Figure 3(a) shows that thermal conductivity decreases for longer wavelength; cumulative thermal conductivities of the SWNT and peapod start to deviate when phonon wavelength $>\sim 1$ nm, which corresponds to the interval of fullerenes in the peapod. The distinct reduction of thermal conductivity in wavelength region of 2–4 nm corresponds to the strong flattening discussed with Fig. 1(e); $q_z a_{\rm lat}/\pi = 0.25$ corresponds to the wavelength of 2.0 nm. As for the frequency dependence, thermal conductivity of CNTs decreases in a wide range of frequency except for 20–30 THz, as shown in Fig. 3(b). While the reduction at around the highest frequency corresponds to the softening of axial modes shown in Fig. 1(b), the large reduction $\sim$10 THz corresponds to the strong flattening of long-wavelength radial modes and hybridization gaps of radial modes discussed with Fig. 1(e). Unlike the impurities that are known to inhibit transport of short-wavelength and high-frequency phonons, it can be observed here that the zone folding of phonon dispersion reduces

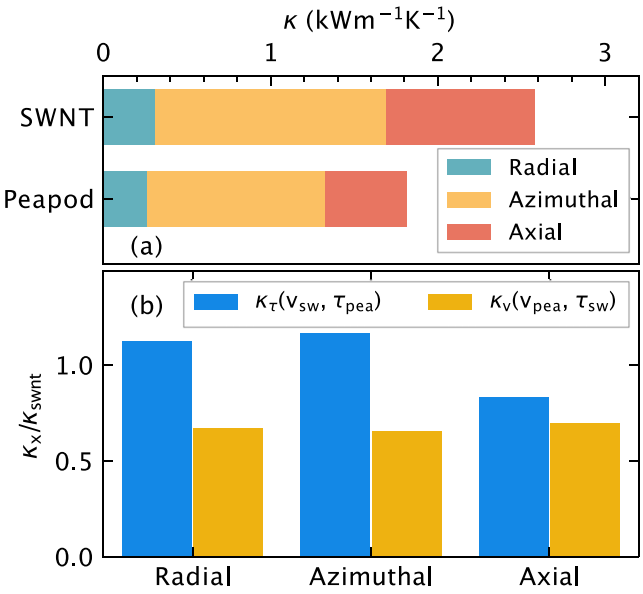

FIG. 4. Decrease in thermal conductivity due to the fullerene encapsulation. (a) Contribution of phonons along each direction, radial, azimuthal, and axial, to thermal conductivity of the single-walled carbon nanotube (SWNT) and peapod. (b) Relative magnitude of influence of relaxation time (blue) and group velocity (orange) to the change of thermal conductivity for phonons along each direction.

the heat transport of phonons with long wavelength and different frequencies including low frequencies.

Figure 4 shows contribution of phonons along each direction: radial (r), azimuthal (θ), and axial (z) direction. To estimate their contribution, thermal conductivity $\kappa(q_z, s)$ is weighted by mean squared displacement along the x direction ($x = r, \theta, z$) of each eigenvector of the SWNT $\boldsymbol{e}_{\rm sw}$, $d(q_z, s; x) = \sum_i |\boldsymbol{e}_{\rm sw}(q_z, s; i, x)|^2$ (see Sec. 5 in the SM [34]), where i is atomic index, and $\boldsymbol{e}_{\rm sw}$ is obtained with lattice dynamics. Figure 4(a) shows that phonons along each direction contribute to heat transport equally for both the SWNT and peapod. This result shows that the fullerene encapsulation affects phonon transport independently of the polarization of phonons.

We now compare the influences of variations in relaxation time and group velocity to the reduction of thermal conductivity. For this, we calculate two different thermal conductivities with either of the group velocity and relaxation time being that of the peapod: $\kappa_{\tau(v)}[v_{\rm sw(pea)}, \tau_{\rm pea(sw)}] = (k_{\rm B}/V) \sum v^2_{g,{\rm sw(pea)}} \tau_{\rm pea(sw)}$. Consequently, we found that the change in the group velocity decreases thermal conductivity by 33%, while the change in the relaxation time increases it by 6%. As shown in Fig. 4(b), the fullerene encapsulation decreases group velocities for any phonon polarization. We therefore conclude that the decrease in group velocity dominates the reduction of thermal conductivity due to the fullerene encapsulation.

We comment on possible issues leading to the discrepancy in the magnitude of thermal conductivity reduction in experiments [30] (≈50%) and our simulations (29%). The most possible reason is the aperiodicity of encapsulated fullerenes in peapods used in the experiment. While fullerenes are encapsulated in every four primitive unit cells of the SWNT in this paper to investigate zone-folding effects, randomness is omnipresent in real materials. Because aperiodic structures, i.e., deviation from the periodicity, leading to wave interference and/or localization can reduce thermal conductivity by more than a few tens of percent compared with periodic structures [47], the discrepancy could be explained with the aperiodic structures in samples used in experiments. Another issue is that, in MD simulations, all phonon modes are equally excited because of the absence of quantum effects and, thus, phonon occupancy cannot be reproduced accurately. Although this is not an issue at room temperature in the case of materials with low Debye temperature, in the case of CNTs whose Debye temperature is much higher than the room temperature [48,49], the contribution of high-frequency phonons to thermal conductivity may be overestimated, resulting in underestimation of the thermal conductivity reduction due to the zone-folding effect that is larger for phonons with lower frequency [see Fig. 3(b)]. While further investigation may be required to clarify this issue, the above issues do not affect our claim; the strain-induced periodic deformation can modulate phonon dispersion and significantly decrease thermal conductivity.

We next decompose the reduction in group velocity to that caused by the uniform and periodic strains. We represent the extent of uniform strain with the change in the difference between the maximum and minimum frequency of each phonon branch $\Delta\omega$ and estimate the group velocity change as $v_{g,\rm uniform} = (\Delta\omega_{\rm pea}/\Delta\omega_{\rm sw})\, v_{g,\rm sw}$. Using this group velocity, the change of thermal conductivity due to the uniform strain field is roughly estimated as $\Delta\kappa_{\rm uniform} = \kappa(v_{\rm g,uniform}, \tau_{\rm pea}) - \kappa_{\rm sw}$, and the rest of the reduction of thermal conductivity $\Delta\kappa_{\rm period} = (\kappa_{\rm pea} - \kappa_{\rm sw}) - \Delta\kappa_{\rm uniform}$ is attributed to the periodic strain field. It is found that 12 and 88% of the decrease in thermal conductivity due to group velocity is attributed to the uniform and periodic strain, respectively. We, thus, conclude that the periodic strain and the resulting zone folding dominate the change of heat transport properties of CNTs at room temperature due to the fullerene encapsulation.

In conclusion, we analyzed the strain effect due to the fullerene encapsulation on phonon properties of CNTs. Our results show that the strain field tunes the wave nature of phonons at room temperature and decreases thermal conductivity of CNTs. The strain effect on group velocity can be divided into the uniform and periodic strain effects. The latter, which leads to zone-folding effects, induces two types of phonons gaps, Bragg gap and hybridization gap, and dominates the change of thermal properties of CNT. Because carbon nanopeapods do not have interface and have a single-nanometer period, they can be an ideal artificial superlattice to tune phonon wave nature. We believe that further experimental study can realize use of coherence wave nature for advanced thermal devices such as thermal rectification [9] and thermal cloaking [10,11].

This work is partially supported by JSPS KAKENHI Grant No. 19H00744, and No. 20K14661 from Japan Society for the Promotion of Science (JSPS), and CREST Grant No. JPMJCR20Q3 and No. JPMJCR19Q3 from Japan Science

and Technology Agency (JST). Numerical calculations in this paper were carried out on the facilities of the Super Computer Center, Institute for Solid State Physics, The University of Tokyo.

[1] J. Shiomi, APL Mater. **4**, 104504 (2016).
[2] M. Maldovan, Nat. Mater. **14**, 667 (2015).
[3] M. Ohnishi and J. Shiomi, APL Mater. **7**, 013102 (2019).
[4] B. Poudel, Q. Hao, Y. Ma, Y. Lan, A. Minnich, B. Yu, X. Yan, D. Wang, A. Muto, D. Vashaee, X. Chen, J. Liu, M. S. Dresselhaus, G. Chen, and Z. Ren, Science **320**, 634 (2008).
[5] D. W. Song, W. N. Shen, B. Dunn, C. D. Moore, M. S. Goorsky, T. Radetic, R. Gronsky, and G. Chen, Appl. Phys. Lett. **84**, 1883 (2004).
[6] K. Esfarjani, G. Chen, and H. T. Stokes, Phys. Rev. B **84**, 085204 (2011).
[7] S. Y. Ren and J. D. Dow, Phys. Rev. B **25**, 3750 (1982).
[8] M. V. Simkin and G. D. Mahan, Phys. Rev. Lett. **84**, 927 (2000).
[9] C. W. Chang, D. Okawa, A. Majumdar, and A. Zettl, Science **314**, 1121 (2006).
[10] T. Han, X. Bai, D. Gao, J. T. L. Thong, B. Li, and C.-W. Qiu, Phys. Rev. Lett. **112**, 054302 (2014).
[11] H. Xu, X. Shi, F. Gao, H. Sun, and B. Zhang, Phys. Rev. Lett. **112**, 054301 (2014).
[12] B. Latour and Y. Chalopin, Phys. Rev. B **95**, 214310 (2017).
[13] A. Jain, Y.-J. Yu, and A. J. H. McGaughey, Phys. Rev. B **87**, 195301 (2013).
[14] N. K. Ravichandran and A. J. Minnich, Phys. Rev. B **89**, 205432 (2014).
[15] M. R. Wagner, B. Graczykowski, J. S. Reparaz, A. El Sachat, M. Sledzinska, F. Alzina, and C. M. Sotomayor Torres, Nano Lett. **16**, 5661 (2016).
[16] J. Lee, W. Lee, G. Wehmeyer, S. Dhuey, D. L. Olynick, S. Cabrini, C. Dames, J. J. Urban, and P. Yang, Nat. Commun. **8**, 14054 (2017).
[17] J. Maire, R. Yanagisawa, A. Ramiere, and S. Volz, Sci. Adv. **3**, e1700027 (2017).
[18] L. Feng, T. Shiga, H. Han, S. Ju, Y. A. Kosevich, and J. Shiomi, Phys. Rev. B **96**, 220301(R) (2017).
[19] J. Ravichandran, A. K. Yadav, R. Cheaito, P. B. Rossen, A. Soukiassian, S. J. Suresha, J. C. Duda, B. M. Foley, C.-H. Lee, Y. Zhu, A. W. Lichtenberger, J. E. Moore, D. A. Muller, D. G. Schlom, P. E. Hopkins, A. Majumdar, R. Ramesh, and M. A. Zurbuchen, Nat. Mater. **13**, 168 (2014).
[20] B. L. Davis and M. I. Hussein, Phys. Rev. Lett. **112**, 055505 (2014).
[21] H. Honarvar and M. I. Hussein, Phys. Rev. B **93**, 081412(R) (2016).
[22] S. Xiong, K. Sääskilahti, Y. A. Kosevich, H. Han, D. Donadio, and S. Volz, Phys. Rev. Lett. **117**, 025503 (2016).
[23] D. Ma, H. Ding, H. Meng, L. Feng, Y. Wu, J. Shiomi, and N. Yang, Phys. Rev. B **94**, 165434 (2016).
[24] J. Lim, K. Hippalgaonkar, S. C. Andrews, A. Majumdar, and P. Yang, Nano Lett. **12**, 2475 (2012).
[25] J. Mendoza and G. Chen, Nano Lett. **16**, 7616 (2016).
[26] R. Anufriev, R. Yanagisawa, and M. Nomura, Nanoscale **9**, 15083 (2017).
[27] J. Lee, H. Kim, S. J. Kahng, G. Kim, Y. W. Son, J. Ihm, H. Kato, Z. W. Wang, T. Okazaki, H. Shinohara, and Y. Kuk, Nature **415**, 1005 (2002).
[28] E. González Noya, D. Srivastava, L. A. Chernozatonskii, and M. Menon, Phys. Rev. B **70**, 115416 (2004).
[29] T. Kawamura, Y. Kangawa, and K. Kakimoto, J. Cryst. Growth **310**, 2301 (2008).
[30] T. Kodama, M. Ohnishi, W. Park, J. Park, T. Shimada, H. Shinohara, and K. E. Goodson, Nat. Mater. **16**, 892 (2017).
[31] T. Okazaki, S. Okubo, T. Nakanishi, S.-K. Joung, T. Saito, M. Otani, S. Okada, S. Bandow, and S. Ijima, J. Am. Chem. Soc. **130**, 4122 (2008).
[32] M. Ashino, D. Obergfell, M. Haluška, S. Yang, A. N. Khlobystov, and R. Wiesendanger, Nat. Nanotechnol. **3**, 337 (2008).
[33] L. Lindsay and D. A. Broido, Phys. Rev. B **81**, 205441 (2010).
[34] See Supplemental Material at http://link.aps.org/supplemental/10.1103/PhysRevB.104.014306 for detailed process of the SED analysis such as extraction of phonon dispersion and relaxation times.
[35] J. Shiomi and S. Maruyama, Phys. Rev. B **73**, 205420 (2006).
[36] Z.-Y. Ong, E. Pop, and J. Shiomi, Phys. Rev. B **84**, 165418 (2011).
[37] X. Li, K. Maute, M. L. Dunn, and R. Yang, Phys. Rev. B **81**, 245318 (2010).
[38] Z. Fan, H. Dong, A. Harju, and T. Ala-Nissila, Phys. Rev. B **99**, 064308 (2019).
[39] D. Donadio and G. Galli, Phys. Rev. Lett. **99**, 255502 (2007).
[40] M. Grujicic, G. Cao, and B. Gersten, Mater. Sci. Eng., B **107**, 204 (2004).
[41] J. Che, T. Çagin, and W. A. Goddard III, Nanotechnology **11**, 65 (2000).
[42] A. Cepellotti, G. Fugallo, L. Paulatto, M. Lazzeri, F. Mauri, and N. Marzari, Nat. Commun. **6**, 6400 (2015).
[43] S. Lee, D. Broido, K. Esfarjani, and G. Chen, Nat. Commun. **6**, 6290 (2015).
[44] S. Huberman, R. A. Duncan, K. Chen, B. Song, V. Chiloyan, Z. Ding, A. A. Maznev, G. Chen, and K. A. Nelson, Science **364**, 375 (2019).
[45] Y. Machida, N. Matsumoto, T. Isono, and K. Behnia, Science **367**, 309 (2020).
[46] S. Lee and L. Lindsay, Phys. Rev. B **95**, 184304 (2017).
[47] S. Ju, T. Shiga, L. Feng, Z. Hou, K. Tsuda, and J. Shiomi, Phys. Rev. X **7**, 021024 (2017).
[48] S. Maruyama, Microscale Thermophys. Eng. **7**, 41 (2010).
[49] J. R. Lukes and H. Zhong, J. Heat Transfer **129**, 705 (2007).